

## Vibrational, magnetic, and dielectric behavior of La-substituted BiFeO<sub>3</sub>-PbTiO<sub>3</sub>

K. K. Mishra, A. T. Satya, A. Bharathi, V. Sivasubramanian, V. R. K. Murthy et al.

Citation: *J. Appl. Phys.* **110**, 123529 (2011); doi: 10.1063/1.3673240

View online: <http://dx.doi.org/10.1063/1.3673240>

View Table of Contents: <http://jap.aip.org/resource/1/JAPIAU/v110/i12>

Published by the [American Institute of Physics](#).

---

### Additional information on J. Appl. Phys.

Journal Homepage: <http://jap.aip.org/>

Journal Information: [http://jap.aip.org/about/about\\_the\\_journal](http://jap.aip.org/about/about_the_journal)

Top downloads: [http://jap.aip.org/features/most\\_downloaded](http://jap.aip.org/features/most_downloaded)

Information for Authors: <http://jap.aip.org/authors>

## ADVERTISEMENT



The advertisement banner features a green and white abstract background with flowing lines. On the left, the text 'AIP Advances' is displayed in a green, sans-serif font, with a series of orange and yellow dots forming an arc above the word 'Advances'. On the right, there is a circular seal with a white border containing the text 'Now Indexed in Thomson Reuters Databases'. Below the main text, a dark blue horizontal bar contains the text 'Explore AIP's open access journal:' in white, followed by a list of three bullet points in white text.

**AIP Advances**

Now Indexed in  
Thomson Reuters  
Databases

Explore AIP's open access journal:

- Rapid publication
- Article-level metrics
- Post-publication rating and commenting

## Vibrational, magnetic, and dielectric behavior of La-substituted BiFeO<sub>3</sub>-PbTiO<sub>3</sub>

K. K. Mishra,<sup>1,a)</sup> A. T. Satya,<sup>1</sup> A. Bharathi,<sup>1</sup> V. Sivasubramanian,<sup>1</sup> V. R. K. Murthy,<sup>1,2</sup> and A. K. Arora<sup>1</sup>

<sup>1</sup>Condensed Matter Physics Division, Indira Gandhi Centre for Atomic Research, Kalpakkam 603102, India

<sup>2</sup>Department of Physics, Indian Institute of Technology Madras, Chennai 600036, India

(Received 26 October 2011; accepted 28 November 2011; published online 30 December 2011)

Phonons and magnetic and ferroelectric ordering in La-substituted (Bi<sub>1-x</sub>La<sub>x</sub>)<sub>0.5</sub>Pb<sub>0.5</sub>Fe<sub>0.5</sub>Ti<sub>0.5</sub>O<sub>3</sub> for samples with 0.0 ≤ x ≤ 0.5 are investigated using Raman, magnetization, and polarization measurements as a function of temperature. The system is tetragonal for pure Bi<sub>0.5</sub>Pb<sub>0.5</sub>Fe<sub>0.5</sub>Ti<sub>0.5</sub>O<sub>3</sub> with a large c/a ratio. The anisotropy is reduced when Bi is partially replaced by La (0 ≤ x ≤ 0.5), and it turns cubic for x ≥ 0.4. All the properties are found to change significantly with changes in the c/a ratio. Evidence of spin-glass-like magnetic ordering at low temperature is found in the case of x = 0.2. A mechanism for the systematic change of magnetic ordering temperature as a function of doping is also discussed. The phonon frequencies and line widths exhibit discontinuous changes across the tetragonal-cubic transition. Large polarization and forbidden Raman scattering in the cubic phase are explained on the basis of symmetry breaking due to the formation of a polar nano region, which leads to relaxor behavior. © 2011 American Institute of Physics. [doi:10.1063/1.3673240]

### I. INTRODUCTION

Multifunctional materials that couple electric, magnetic, and structural order parameters to result in the coexistence of ferroelectric, ferromagnetic, and ferroelastic behaviors have attracted considerable attention in the scientific community in recent years. Rhombohedral BiFeO<sub>3</sub> (BF) is unique among multiferroic materials due to the coexistence of two types of long-range order: antiferromagnetic order below the Neel temperature  $T_N = 643$  K, and ferroelectric order below the Curie temperature  $T_C = 1100$  K.<sup>1,2</sup> However, the compound was not found to show the magnetoelectric effect, as an spiral modulated spin structure led to the disappearance of the overall magnetization.<sup>3</sup> In addition, the electric polarization was found to be quite low.<sup>4,5</sup> Furthermore, the synthesis of an ideal perovskite phase of pure BF is difficult because of the comparable thermodynamic stability of Fe<sup>3+</sup> and Fe<sup>2+</sup> states of iron in this compound.<sup>6,7</sup> In order to overcome these limitations, several solid-solutions have been synthesized, and their properties have been investigated. The solid-solutions of BF with other ABO<sub>3</sub> compounds such as PbTiO<sub>3</sub> (PT), PrFeO<sub>3</sub>, and BaTiO<sub>3</sub> stabilize the perovskite phase and exhibit spontaneous magnetization.<sup>8-10</sup> Recently, Zhu *et al.* have carried out structural and magnetic studies on (1-y)(BiFeO<sub>3</sub>)-y(PbTiO<sub>3</sub>) solid solutions as a function of composition.<sup>11</sup> It was pointed out that mixed crystals with a BiFeO<sub>3</sub>-PbTiO<sub>3</sub> (BF-PT) ratio of around 50:50 favor the formation of chemically ordered micro-regions in which the spiral spin modulation decreases. Singh *et al.*<sup>12</sup> reported improved dielectric and magneto-electric properties in the system 0.50(Bi<sub>1-x</sub>La<sub>x</sub>FeO<sub>3</sub>)-0.50(PbTiO<sub>3</sub>) for compositions

with x = 0.5. However, the phonon spectra of this system were not investigated. In addition, the dependence of phonon, magnetic, and dielectric behaviors on La-substitution have not been reported so far. Cheng *et al.*<sup>13</sup> studied the effect of La-doping on the magnetic and electrical behavior of 0.45(Bi<sub>1-x</sub>La<sub>x</sub>FeO<sub>3</sub>)-0.55(PbTiO<sub>3</sub>) only in the limited range of 0.1 ≤ x ≤ 0.3 and found significantly enhanced polarization and magnetization as compared to that in pure BiFeO<sub>3</sub>. In order to study this system over a wider range of compositions, we have recently synthesized the 0.50(Bi<sub>1-x</sub>La<sub>x</sub>FeO<sub>3</sub>)-0.50(PbTiO<sub>3</sub>) (BLFPT<sub>x</sub>) solid-solution with a composition range of x = 0.0–0.5 and found it to be in a cubic structure (*Pm3m*) for x ≥ 0.4 and tetragonal (*P4mm*) for x < 0.4, based on analysis of x-ray diffraction data.<sup>14</sup> Furthermore, the dependence of the tetragonal-cubic transition temperature ( $T_{T-C}$ ) on the La-composition x shows that at higher x the transition occurs at lower temperatures.<sup>15</sup> The phonon spectra of pure and La-substituted BF-PT have not been investigated as a function of temperature or across the tetragonal-cubic transition. Raman spectroscopy is a powerful technique for studying short-range order<sup>16-19</sup> and phase transitions in perovskites.<sup>16,20-22</sup> The phonon dynamics can provide useful insight into microscopic properties such as mode softening, structure property relations, the nature of local ordering, and structure in the nano-scale range.<sup>23,24</sup>

The BLFPT<sub>x</sub> solid solution belongs to the family of perovskite structures with the general formula ABO<sub>3</sub> (see the inset of Fig. 1). The sublattice A is occupied by randomly distributed nonmagnetic Bi<sup>3+</sup> (6p<sup>0</sup>, S = 0), Pb<sup>2+</sup> (6p<sup>0</sup>, S = 0), and La<sup>3+</sup> (5d<sup>0</sup>, S = 0) ions, and the B site is occupied by randomly distributed magnetic Fe<sup>3+</sup> (3d<sup>5</sup>, S = 5/2) and nonmagnetic Ti<sup>4+</sup> (3d<sup>0</sup>, S = 0) ions. Incorporating La<sup>3+</sup> and Pb<sup>2+</sup> cations at the Bi<sup>3+</sup> site and Ti<sup>4+</sup> at the Fe<sup>3+</sup> site can cause a canted spin arrangement of unpaired electrons on Fe<sup>3+</sup> ions.<sup>25</sup> It is also argued that La<sup>3+</sup> doping in BF destroys

<sup>a)</sup>Authors to whom correspondence should be addressed. Electronic addresses: kkm@igcar.gov.in and karuna\_phy05@yahoo.co.in. Fax: +91-44-27480081.

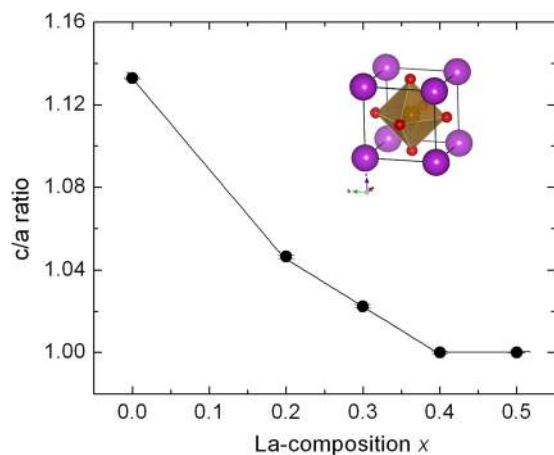


FIG. 1. (Color online) Variation of  $c/a$  ratio for  $(\text{Bi}_{1-x}\text{La}_x)_{0.5}\text{Pb}_{0.5}\text{Fe}_{0.5}\text{Ti}_{0.5}\text{O}_3$  ( $0 \leq x \leq 0.5$ ) with composition  $x$ . The line connecting the data points is a guide for the eye. The inset shows the  $\text{ABO}_3$  perovskite structure displaying a  $\text{BO}_6$  octahedron.

the spiral modulated spin structure and favors a collinear antiferromagnetic spin configuration.<sup>26</sup> In addition, BF-PT possesses a strong chemical inhomogeneity due to the occupation of  $A$  and  $B$  sites by heterovalent cations. This leads to a frustration between charge neutrality and lattice strain, which on the local scale can result in the formation of an ordered nanoregion.<sup>27,28</sup> There are a few reports of investigations of the magnetic and polarization behaviors of La-modified  $\text{BiFeO}_3$ - $\text{PbTiO}_3$  with different ratios of BF and PT. However, there is no systematic study on the effect of La on the evolution of magnetic and polarization behaviors of  $\text{BLFPT}_x$  in the full range of  $x$ . In the present work, phonons and magnetic and ferroelectric ordering in La-substituted  $\text{BLFPT}_x$  are investigated for samples with  $x = 0.0, 0.2, 0.3, 0.4$ , and  $0.5$  using Raman, magnetization, and polarization measurements as a function of temperature. The Raman spectra are analyzed quantitatively in order to obtain mode frequencies and their line widths and intensities. Magnetization measurements are made from ambient down to 4 K in field-cooled and zero-field-cooled conditions. The field dependence of magnetization is also studied in order to examine the possibility of a spin-glass-like magnetic ordering. From the ferroelectric hysteresis loop, the composition dependence of the remanent polarization is also obtained. The observed results are discussed in the context of anisotropy and tetragonal-cubic structural transition.

## II. EXPERIMENTAL DETAILS

Polycrystalline  $(\text{Bi}_{1-x}\text{La}_x)_{0.5}\text{Pb}_{0.5}\text{Fe}_{0.5}\text{Ti}_{0.5}\text{O}_3$  powder samples were synthesized for  $x = 0.0, 0.2, 0.3, 0.4$ , and  $0.5$  using the solid-state reaction technique. The high purity precursors ( $\text{Bi}_2\text{O}_3$ ,  $\text{La}_2\text{O}_3$ ,  $\text{PbO}$ ,  $\text{Fe}_2\text{O}_3$ , and  $\text{TiO}_2$ ) of 99.9% purity (Alfa Aesar), weighed in stoichiometric proportion, were mixed using an agate mortar for 2 h and then in a wet (acetone) medium for 4 h to get a homogeneous mixture. The mixtures so obtained were then calcined in a closed platinum crucible for 3 h at 773 K in air, reground, and calcined again for 4 h at 1073 K. The calcined powders were pressed

into pellets and sintered at 1373 K for 2 h. The pellets were about 10.5 mm in diameter and 1.5 mm thick. The formation and quality of the compounds were checked via x-ray diffraction analysis. The x-ray powder diffraction patterns of the sintered samples were measured in order to determine the structure and confirm the phase purity.  $\text{Cu-K}\alpha$  radiation was used to record the diffraction patterns with a Siemens x-ray diffractometer (D500) operating in the Bragg-Brentano geometry. Diffraction patterns were analyzed using *STOE* software for indexing the peaks and obtaining the refined lattice parameters. Energy dispersive x-ray analysis (EDAX) and microstructural analysis (i.e., grain size, grain distribution, voids, etc.) of the samples were carried out using a Cam Scan (CS 3200) scanning electron microscope. Selected area electron diffraction (SAED) patterns were obtained using a JEOL-2000 EX II transmission electron microscope operated at 200 kV. Raman spectra were recorded using a Ranishaw micro-Raman spectrometer (model: InVia) equipped with a Leica microscope and a  $20\times$  long-working distance objective. The measurements were conducted in backscattering geometry using the 514.5 nm line of an Ar-ion laser. The spectrometer resolution for 1800 l/mm grating was  $\sim 2\text{ cm}^{-1}$ . *In situ* temperature-dependent experiments were conducted in a Linkam heating-cooling stage ensuring a temperature stability of  $\pm 0.1\text{ K}$ . The data acquisition time and the laser power were adjusted so as to obtain a good signal-to-noise ratio. The spectra were fitted to Lorentzian line shapes to determine the peak positions, full widths at half maximum, and intensities using *PEAKFIT* software (*JANDEL*). Magnetizations ( $M$ - $H$  loop) were obtained using a vibrating sample magnetometer (VSM-ADE, model EV9) up to a maximum field of  $\pm 50\text{ kOe}$  at ambient and down to 4 K. The zero field cooled (ZFC) and field cooled (FC) magnetization were measured as a function of  $T$  in the 4–300 K range. For  $P$ - $E$  measurements, the pellets were silver electroded on both sides. The  $P$ - $E$  measurements were carried out using an automatic  $P$ - $E$  loop tracer.

## III. RESULTS AND DISCUSSION

### A. Structural and microstructural properties

The x-ray diffraction results indicate the formation of a single-phase Perovskite structure for all La-substituted BF-PT samples ( $0 \leq x \leq 0.5$ ). For the sample with  $0 \leq x \leq 0.3$ , the systems show a tetragonal structure ( $P4mm$ ), and for  $x \geq 0.4$ , the tetragonal distortion disappears and the system shows a cubic structure ( $Pm3m$ ).<sup>14</sup> With La-substitution there is a slight increase in the  $a$  lattice parameter, whereas the lattice parameter  $c$  decreases rapidly. Figure 1 shows the monotonic change in lattice anisotropy ( $c/a$ ) from 1.133 to 1 as a function of La-composition. EDAX measurements were carried out on pellets of all the samples in order to study the chemical composition. The EDAX spectra (Fig. 2) of the samples show the presence of all the cationic elements. Scanning electron micrographs (inset of Fig. 2) taken of the fractured surfaces of pellets show a uniform distribution of grains throughout the surface of the sample. The grain size is slightly different for each La-content, but there is no correlation between the two parameters. The density of all

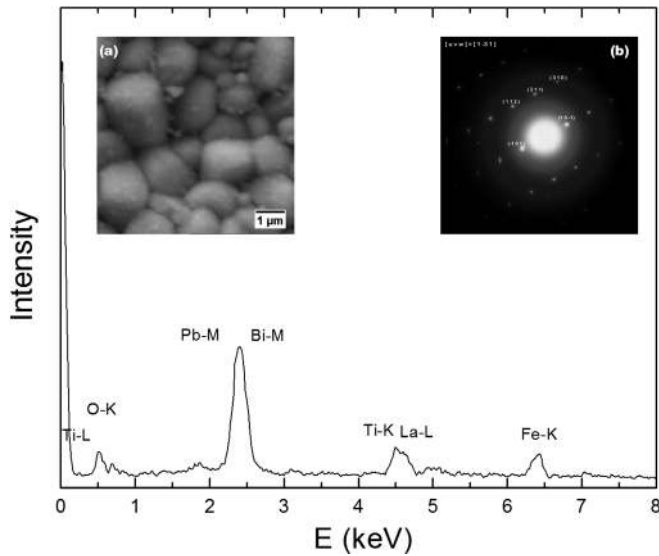


FIG. 2. EDAX spectra of BLFPT<sub>x</sub> sample with  $x=0.4$ . Inset (a) shows the scanning electron micrograph. Inset (b) is the selected area diffraction pattern confirming the cubic phase. Zone axis  $[u\ v\ w] = [1\ \bar{3}\ 1]$ .

samples was between 96.5% and 99% of the theoretical density. Table I gives the characteristic parameters of the microstructure and the tetragonal-cubic phase transition temperature for the samples. The selected area diffraction patterns indicate the polycrystalline nature of all samples and are indexed to the tetragonal phase for  $0 \leq x \leq 0.3$  and cubic for  $x \geq 0.4$  (inset of Fig. 2).

TABLE I. Compositional dependence of the grain size, relative density, and tetragonal-cubic transition temperature ( $T_{T-C}$ ) for BLFPT<sub>x</sub> ( $0 \leq x \leq 0.5$ ).

$x$ -La	0	0.2	0.3	0.4	0.5
Grain size ( $\mu\text{m}$ )	0.95	1.2	1.15	1.5	1.2
Relative density	96.5%	97%	99%	99%	99%
$T_{T-C}$ <sup>a</sup>	715 °C	500 °C	345 °C	Cubic	Cubic

<sup>a</sup>Data from Ref. 15.

## B. Raman scattering

The tetragonal phase of pure and La-substituted BF-PT belongs to the same space group as that of PbTiO<sub>3</sub>; therefore the same set of irreducible representations of the phonons is applicable here. These are  $\Gamma_{\text{opt}} = 3A_1 + 4E + B_1$ , where the  $A_1$  and  $E$  modes are both Raman and infrared active, and the  $B_1$  mode is Raman active only. The Raman spectra were found to be broad at ambient temperature. The Raman lines are known to become narrow, and the overlapping peaks better resolved, at low temperature due to an increase in the phonon life-times. In order to confirm whether the broad nature of the Raman bands was intrinsic to this mixed crystal system or due to the finite (ambient) temperature of the measurement, Raman spectra of all the compositions were also recorded at 83 K. Figure 3(a) shows the Raman spectra for all the compositions ( $0 \leq x \leq 0.5$ ) at 83 K. All the major peaks became slightly narrower as compared to those at ambient temperature. In addition, some of the weak bands that existed as shoulders at ambient became prominent.

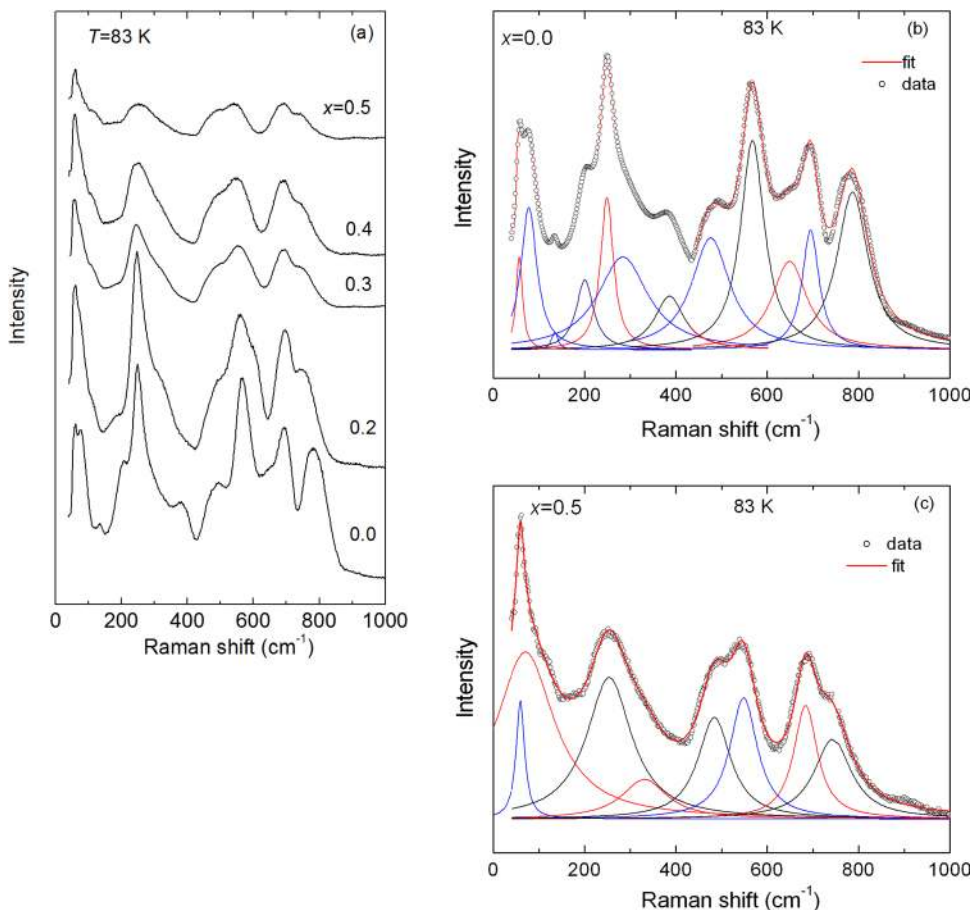


FIG. 3. (Color online) Raman spectra of BLFPT<sub>x</sub> recorded at 83 K (a) for  $0 \leq x \leq 0.5$ . (b) Fitted spectrum for  $x=0.0$ . Individual fitted peaks are also shown. (c) Fitted spectrum for  $x=0.5$ . Individual fitted peaks are also shown.

TABLE II. Mode frequencies in BLFPT<sub>x</sub> ( $0 \leq x \leq 0.5$ ) at 83 K.

Mode frequency ( $\text{cm}^{-1}$ )					Assignment <sup>a</sup>
$x = 0.0$	$x = 0.2$	$x = 0.3$	$x = 0.4$	$x = 0.5$	
57	...	58	...	59	E-TA
78	64	82	64	70	E <sup>(1)</sup> -TO
134	135	...	...	...	E <sup>(1)</sup> -LO
200	...	...	...	...	A <sub>1</sub> <sup>(1)</sup> -TO
249	247	243	244	253	E <sup>(2)</sup> -TO
283	304	290	296	330	E <sup>(4)</sup> -TO
386	...	...	...	...	A <sub>1</sub> <sup>(2)</sup> -TO
476	482	479	482	484	E <sup>(2)</sup> -LO
568	564	556	552	548	E <sup>(3)</sup> -TO
648	...	...	...	...	A <sub>1</sub> <sup>(2)</sup> -LO
695	694	688	684	684	A <sub>1</sub> <sup>(3)</sup> -TO
786	758	751	741	743	E <sup>(3)</sup> -LO

<sup>a</sup>Assignment of modes in the tetragonal phase is based on the comparison with mode frequencies of PbTiO<sub>3</sub> (Ref. 29).

A quantitative analysis of the changes in the Raman spectra is possible only when the peak positions, line-widths, and intensities of the modes are precisely obtained using curve fitting. Therefore, the spectra were fitted to multi-Lorentzians using the PeakFit program. The individual components and total fitted spectrum for  $x = 0.0$  and  $0.5$  are shown in Figs. 3(b) and 3(c), respectively. Similar fittings have been done for other compositions. For  $x = 0.0$ , the fitting, yielding 12 peaks, is shown in Fig. 3(b), whereas 8 peaks could be identified in the case of  $x = 0.5$ . One can see good agreement between the total fitted spectrum and the data. Table II gives the frequencies of the Raman modes at 83 K and their assignments<sup>29</sup> for all the compositions. One can see that the mode frequencies do not depend strongly on the composition of La; however, some of the weak modes are not present in the mixed-crystals with higher values of  $x$ .

Figure 4 shows the Raman spectra of pure and La-substituted BF-PT samples at elevated temperature, from ambient to 873 K. At ambient temperature, in pure BF-PT (Fig. 4(a)) five prominent broad peaks and several shoulders are observed, similar to the spectrum at 83 K. The broad nature of the Raman peaks recently has been argued to arise due to substitutional disorder at cation sites A and B.<sup>14</sup> In La-substituted BF-PT, the peaks are found to be broader than those of pure BF-PT, and their intensities are low even at ambient (Figs. 4(b) and 4(c)). This is discussed in more detail further on in the paper. One can see from Fig. 4 that at elevated temperatures, the spectra broaden further, and the intensities are found to decrease. These spectra were also analyzed using Lorentzian fitting. The fittings of 298 and 673 K Raman spectra of pure BF-PT are shown in Fig. 5. One can see that the 134, 200, 386, and 476  $\text{cm}^{-1}$  bands of the 83 K spectrum become weaker and appear as shoulders. Similar to that obtained at 83 K, the spectrum at 298 K could be resolved into a total of 12 peaks. At 673 K, the shoulders at 200 and 385  $\text{cm}^{-1}$  disappear, and only 10 modes could be fitted to the spectrum. In the context of the number of peaks used to fit the spectrum for a given composition or temperature, it is important to point out that although it is always

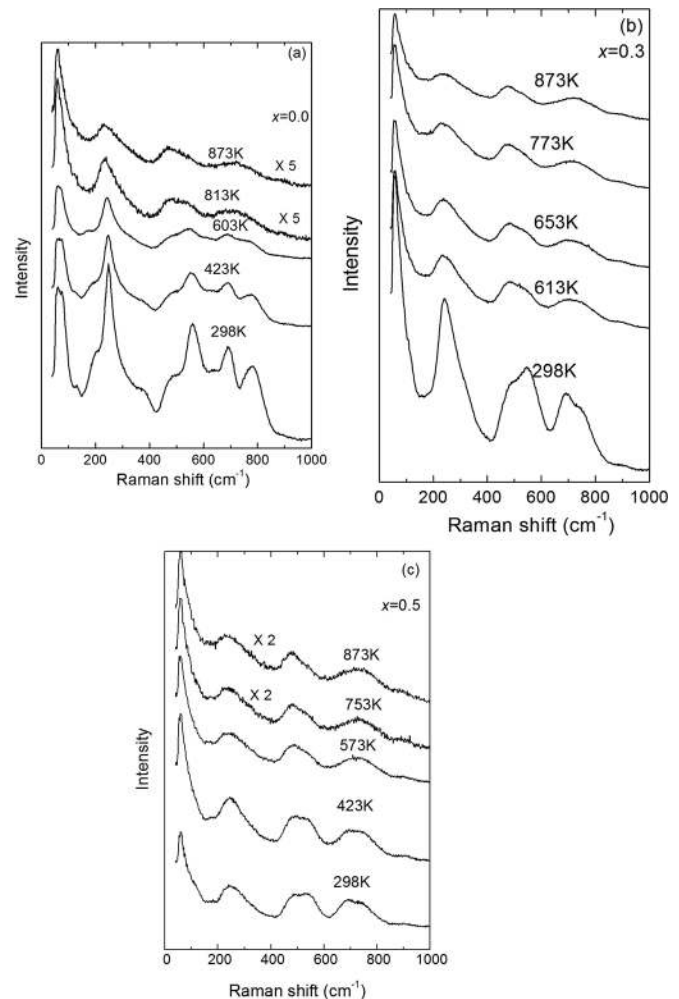


FIG. 4. Temperature evolution of Raman spectra of  $(\text{Bi}_{1-x}\text{La}_x)_{0.5}\text{Pb}_{0.5}\text{Fe}_{0.5}\text{Ti}_{0.5}\text{O}_3$  for (a)  $x = 0.0$ , (b)  $x = 0.3$ , and (c)  $x = 0.5$ .

possible to fit a greater number of peaks to a given spectrum, we adopted a strategy in which we use the minimum number of peaks that yields a good fit. If one uses more modes than required, it leads to large standard errors and strong correlations in fitted parameters. At 873 K, the modes at 134, 200, 283, 386, 648, and 786  $\text{cm}^{-1}$  could not be identified (Fig. 4(a)), and thus only 6 modes survived at the highest temperature. The lower number of modes at high temperature is a result of the insufficient intensity of weak bands.

In samples with  $x = 0.2$  and  $0.3$ , 8 modes were found at ambient. Similar to the sample with  $x = 0$ , the modes broaden with increasing temperature, as expected, and as many as 5 modes survived at 873 K. As mentioned earlier, pure BF-PT is tetragonal ( $P4mm$ ) at ambient temperature<sup>14</sup> and transforms to the cubic phase ( $Pm3m$ ) at 993 K.<sup>15</sup> Therefore, the structural transition temperature is higher than the highest temperature reached in the present measurements. The occurrence of a smaller number of modes at the highest temperature is essentially due to the broadening and weakening of modes that could not be identified in the fitting procedure. In the substituted mixed-crystals, the tetragonal anisotropy decreases at elevated temperatures and for  $x = 0.2$  and  $0.3$ , and the system transforms to the cubic phase ( $Pm3m$ ) at 813 and 618 K, respectively.<sup>15</sup> These transition

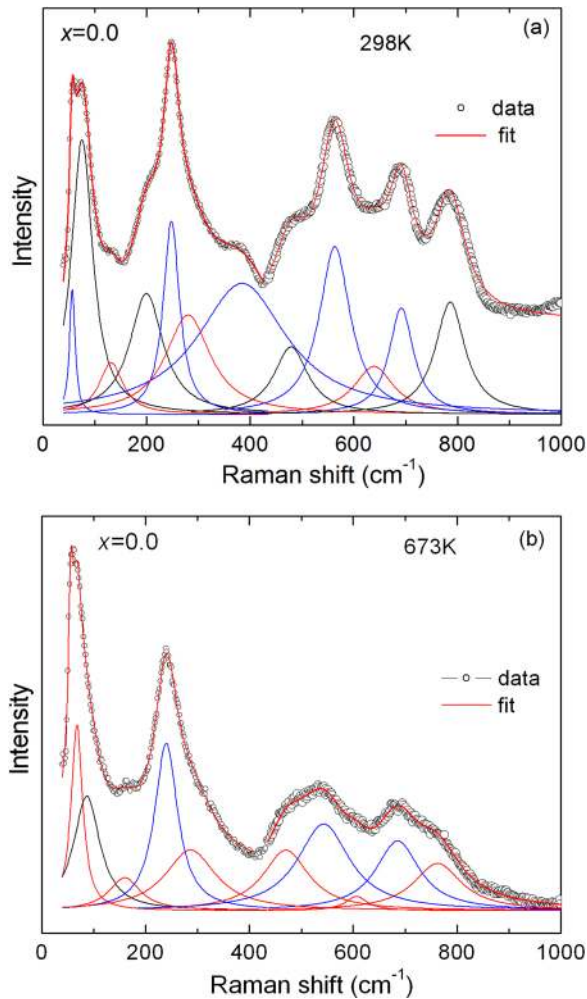


FIG. 5. (Color online) Raman spectrum fitted to the sum of Lorentzian peaks for  $x=0.0$  (a) at 298 K and (b) at 673 K. Individual fitted peaks are also shown.

temperatures are lower than the highest temperature in the present investigations, and as a result it is possible that certain anomalies in the temperature dependence of the parameters of the modes could exist across the structural transition. An analysis of parameters such as Raman mode frequencies and line-widths will be discussed later from the point of view of identification of the phase transition. At ambient, upon La-substitution the system becomes cubic ( $Pm3m$ ) for  $x \geq 0.4$ .<sup>14</sup> The evolution of the Raman spectrum at elevated temperature is shown in Fig. 4(c) for  $x=0.5$ . For  $x=0.4$  and 0.5, as many as 7 modes are observed at ambient. All modes are broad, and only 4 modes could be found at 873 K.

The irreducible representation for the optical phonons in the cubic phase is  $\Gamma_{\text{opt}} = 3F_{1u} + F_{2u}$ , where the  $F_{1u}$  mode is infrared active and  $F_{2u}$  is a “silent mode,” because it is inactive both in the Raman and in the infrared.  $A_1$  and E modes of the tetragonal phase combine to give the  $F_{1u}$  mode of the cubic phase. Similarly,  $B_1$  and E modes combine to give  $F_{2u}$ . The splitting of  $A_1$  and E modes is found to decrease as the anisotropy decreases upon La substitution.<sup>14</sup> Thus, the appearance of weak Raman spectra in samples with  $x=0.4$  and 0.5 has been attributed to the breakdown of Raman selection rule due to substitutional disorder at the cation

sites, because the mode frequencies in the cubic phase continued to correspond with those in the tetragonal phase. The spectra for these compositions are likely to have a large contribution from the phonon density of states. Appearance of features corresponding to the phonon density of states are well known to appear along with zero-center phonon Raman lines, even in single crystals of the homogeneous solid solution (mixed crystals).<sup>30</sup> In fact, the flat regions of the dispersion curves near the zone center and other high symmetry points in the Brillouin zone make a large contribution to the phonon density of states. Thus, all the phonons, whether Raman active or not, can, in principle, contribute to the disorder activated Raman scattering, as found in samples with  $x=0.4$  and 0.5. The appearance of Raman spectra in the cubic phase has also been interpreted as evidence of symmetry breaking. This is argued to arise due to the existence of nanoscale ordering (polar nano regions), which is not detectable with x-ray diffraction.<sup>27</sup> In certain substituted compounds, local chemical ordering gives additional sharp Raman lines<sup>27</sup> riding over the broad spectrum; however, in the present system we do not find such additional peaks.

Figure 6 shows the dependence of mode frequencies on temperature. One can see that the frequencies of almost all the modes decrease with increasing temperature. This is understandable on the basis of the anharmonicity of phonons.<sup>31</sup> For  $x=0.0$ , the modes at 131, 199, and 638  $\text{cm}^{-1}$  vanish at a temperature of around 700 K. The mode pairs at 279 and 384  $\text{cm}^{-1}$  and 695 and 786  $\text{cm}^{-1}$  merge and give rise to single peaks (Fig. 6(a)). Similarly, in the case of  $x=0.2$ , only 5 modes survived at 873 K (Fig. 6(b)). The weak mode at 176  $\text{cm}^{-1}$  vanishes and the modes at 246 and 290  $\text{cm}^{-1}$  and 692 and 765  $\text{cm}^{-1}$  merge to give rise to single peak each. One can notice from Fig. 6(c) that the mode at 291  $\text{cm}^{-1}$  disappears and the modes at 684 and 740  $\text{cm}^{-1}$  merge and show a single mode at  $\sim 620$  K, which is close to the tetragonal-cubic phase transition temperature of 618 K for the  $x=0.3$  system. In principle, one can expect signatures of the structural transition for the  $x=0.2$  system also; however, if we compare Fig. 6(b) with Fig. 6(c), we see that the 290 and 692  $\text{cm}^{-1}$  modes, which disappeared at 618 K in the compound with  $x=0.3$ , are already absent in the compound with  $x=0.2$  well below the transition temperature of 813 K due to weak intensity. The five modes that are present above 618 K in the sample with  $x=0.3$  also exist when  $x=0.2$  over a wide temperature range. As a result, those signatures of the phase transition are not found when  $x=0.2$  at temperatures near 813 K. Figures 6(d) and 6(e) show the merging of modes at 285, 479, and 682  $\text{cm}^{-1}$  with those at 239, 544, and 739  $\text{cm}^{-1}$ . The line-widths of almost all modes are found to increase with increasing temperature. This is expected due to reduced phonon life times at elevated temperature. However, a few modes exhibit the opposite behavior, i.e., they become narrow at high temperature. The temperature dependence of the line-widths of the pair of modes at 488 and 551  $\text{cm}^{-1}$  is shown in Fig. 7 for  $x=0.3$ . It may be pointed out that in the  $x=0.3$  system, the neighboring modes at 386 and 648  $\text{cm}^{-1}$  (found in  $x=0$ ) are not found even at 83 K. Thus, the line-width parameters of 488 and 551  $\text{cm}^{-1}$  are not expected to be affected by other far-away peaks, and

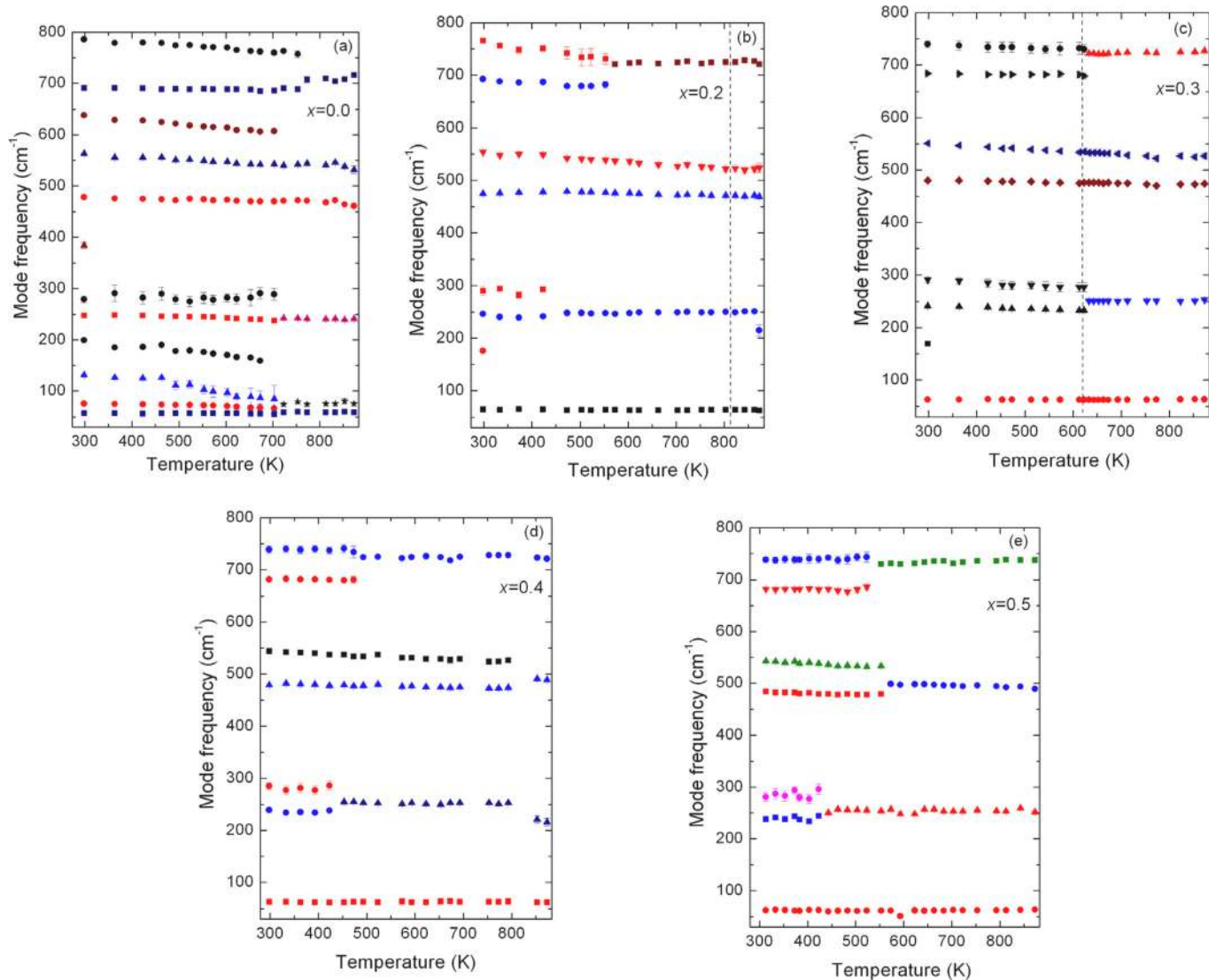


FIG. 6. (Color online) Dependence of Raman mode frequencies on temperature for (a)  $x=0.0$ , (b)  $x=0.2$ , (c)  $x=0.3$ , (d)  $x=0.4$ , and (e)  $x=0.5$ . Vertical dashed lines correspond to tetragonal-cubic transition.

the temperature dependence presented in Fig. 7 is genuine. The line-widths of these modes also show an anomaly around 618 K associated with the tetragonal-cubic phase transition. These modes are associated with the oxygen vibrations of  $\text{BO}_6$  octahedral. As the temperature is increased, the anisotropy of the octahedral decreases. As a result, the distribution of B-O bond lengths is expected to decrease. This can reduce the inhomogeneous broadening of the octahedral vibrations. It may be pointed out that the homogeneous (intrinsic) broadening of phonons in pure compounds is much smaller at ambient and even at elevated temperature than the inhomogeneous broadening in mixed crystals due to bond-length distribution. For example, in pure  $\text{BiFeO}_3$  the two Fe-O distances are 1.958 and 2.110 Å, whereas in pure  $\text{PbTiO}_3$  the two Ti-O distances are 1.97 and 2.032 Å. Thus, in the sample with  $x=0.3$ , the B-O bond lengths in  $\text{BO}_6$  octahedral are expected to have a range of values. At ambient, the average B-O bond length in the  $a$ - $b$  plane is 1.966 Å, and along the  $c$ -direction it is 2.01 Å. In the cubic phase, the  $\text{BO}_6$

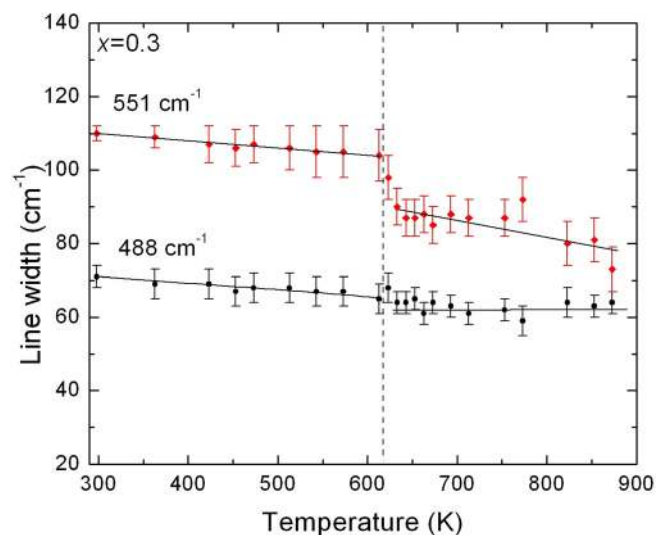


FIG. 7. (Color online) Dependence of Raman line-widths on temperature for  $x=0.3$ . Lines through the data points show the change in slope. The vertical dashed line at 618 K corresponds to the phase transition.

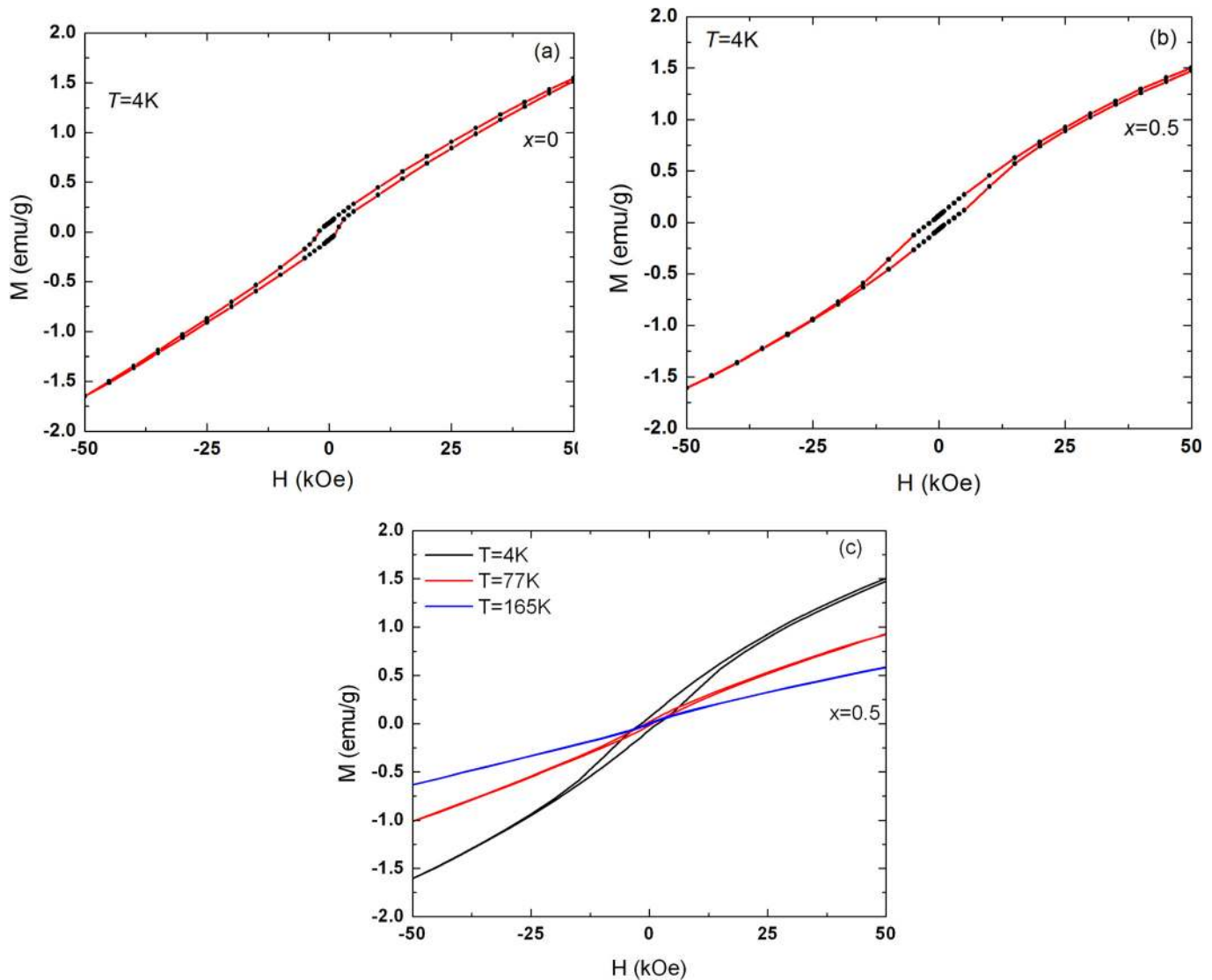


FIG. 8. (Color online) Magnetic hysteresis loop of  $(\text{Bi}_{1-x}\text{La}_x)_{0.5}\text{Pb}_{0.5}\text{Fe}_{0.5}\text{Ti}_{0.5}\text{O}_3$  (a) for  $x=0.0$  at 4 K, (b) for  $x=0.5$  at 4 K, and (c) for  $x=0.5$  at different temperatures.

octahedron becomes regular with a bond length of 1.983 Å. A regular octahedron is expected to have a narrow distribution of bond lengths.

### C. Magnetic behavior

Figures 8(a) and 8(b) present the results of magnetization measurements at 4 K, showing the hysteresis loops in the  $M$ - $H$  curves for  $x=0$  and 0.5, respectively. Other compositions also show similar behavior. The present results for  $x=0$  are similar to those reported by Zhu *et al.*<sup>11</sup> for the 45:55 BF-PT system. The value of the magnetization obtained in the present sample is more than that reported previously.<sup>11</sup> The  $M$ - $H$  curves for all compositions show a hysteresis loop, and it does not saturate with applied fields of up to 6 T. From the hysteresis loop, it can be inferred that magnetization arises because of two contributions. One is the ferromagnetic contribution, which gives the hysteresis curve, and the other is the paramagnetic host, which gives rise to a linear variation of  $M$  at higher field. This suggests the

existence of magnetically ordered clusters in an overall paramagnetic host. The formation of magnetically ordered clusters in solid solutions has been reported in other systems also.<sup>11</sup> The remanent magnetization appears to depend on  $x$ . This has been argued to be due to the incorporation of  $\text{La}^{3+}$  in the  $A$  site of  $\text{BLFPT}_x$  leading to the destruction of the spiral modulated spin structure and thereby enhancing Dzyaloshinskii-Moriya type interaction.<sup>25,26</sup> The  $M$ - $H$  loop for  $x=0.5$  at different temperatures is shown in Fig. 8(c). A hysteresis loop with remanent magnetization appears clearly at 77 K and becomes more enhanced at 4 K. However, at room temperature all samples are in a paramagnetic state.

In order to understand the nature of the magnetic ordering, the temperature dependence of the magnetization was investigated at an applied field of 1 kOe for all the samples. For ZFC magnetization measurement, the sample is cooled from room temperature to 4 K without any external magnetic field, and the magnetization is recorded while the sample is heated in the applied field of 1 kOe. In case of FC magnetization, the sample is cooled under the same magnetic

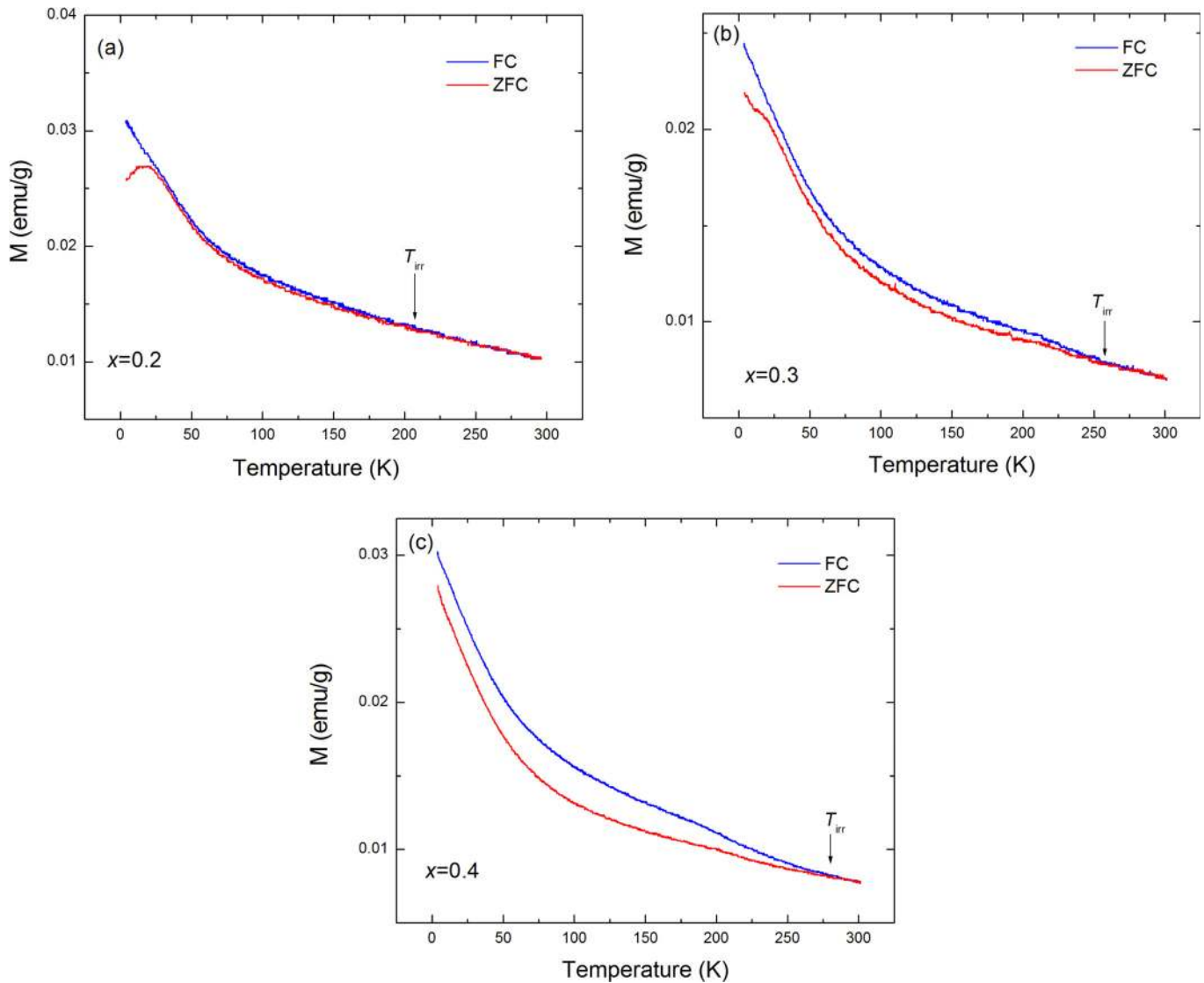


FIG. 9. (Color online) Dependence of FC and ZFC magnetization of  $(\text{Bi}_{1-x}\text{La}_x)_{0.5}\text{Pb}_{0.5}\text{Fe}_{0.5}\text{Ti}_{0.5}\text{O}_3$  at constant static applied magnetic field of 1 kOe for (a)  $x=0.2$ , (b)  $x=0.3$ , and (c)  $x=0.4$ .

field, and the magnetization is measured. Figure 9 shows the temperature dependence of ZFC and FC magnetization at a static field of 1 kOe. One can see that the magnetization decreases with temperature and depends on the thermal history of the samples exhibiting an irreversibility effect. The temperature at which the irreversible magnetization  $M_{\text{irr}}$  ( $M_{\text{irr}} = M_{\text{FC}} - M_{\text{ZFC}}$ ) becomes nonzero is called the irreversibility temperature ( $T_{\text{irr}}$ ); this is where the ZFC and FC branches coalesce. The  $T_{\text{irr}}$  is found to shift toward higher temperature with increasing La-composition. This will be discussed later in more detail.

It may be pointed out that for the sample with  $x=0.2$ , the ZFC magnetization shows a cusp at low temperature. This could be due to a spin glass behavior.<sup>27,32</sup> In order to confirm this, the ZFC magnetization was measured at different static applied magnetic fields, and the dependence of the peak temperature on the applied field was obtained. Figure 10(a) shows the temperature dependence of ZFC magnetization for  $x=0.2$  at different static applied fields. One can see that at 1 kOe, the peak of the magnetization

curve occurs around 17.5 K, the spin glass transition temperature  $T_g$ . The peak position  $T_g$  shifts to lower temperature at higher fields and gradually broadens. A shift of  $T_g$  with field is one of the characteristic features of a spin-glass-like behavior.<sup>32–36</sup> A spin glass order parameter can be estimated from the field dependence of  $T_g(H)$  that vanishes linearly with temperature at the freezing temperature ( $T_F$ ).<sup>34</sup> It can be pointed out that a spin glass is described by many order parameters, and not by a single one, because of the existence of many phases.<sup>35</sup> In order to understand the frozen state and freezing transition, the behavior of magnetic field has been analyzed in the field-temperature plane ( $T_g$  versus  $H^{2/3}$  and  $T_g$  versus  $H^2$ ). In Figs. 10(b) and 10(c), the field dependence of  $T_g$  is analyzed with  $H^{2/3}$  and  $H^2$  dependence for comparison with the critical line predicted by de Almeida and Thouless (called the AT line) for Ising spin glass and that predicted by Gabay and Toulouse (called the GT line) for the Heisenberg spin glass.<sup>32–35</sup> As can be seen, the data fit well with the AT line, implying an Ising spin glass, and  $T_F$  was found to be  $18.6 \pm 0.2$  K. The exact nature of the frozen

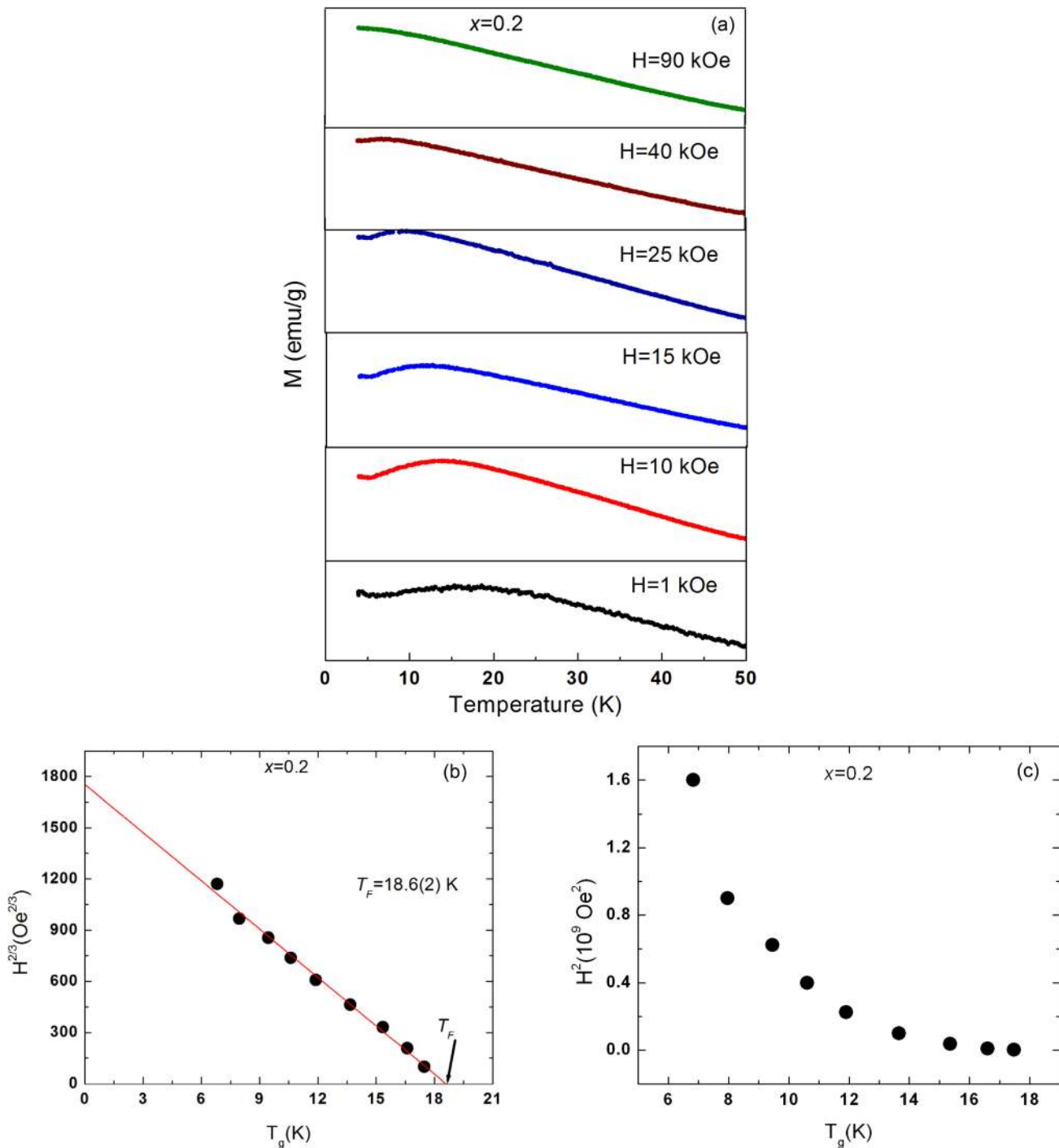


FIG. 10. (Color online) (a) ZFC curves of  $(\text{Bi}_{1-x}\text{La}_x)_{0.5}\text{Pb}_{0.5}\text{Fe}_{0.5}\text{Ti}_{0.5}\text{O}_3$ ,  $x=0.2$ , in different applied magnetic fields. (b) Field ( $H$ ) dependence of  $T_g$  raised to powers of  $2/3$  and  $2$  for  $(\text{Bi}_{1-x}\text{La}_x)_{0.5}\text{Pb}_{0.5}\text{Fe}_{0.5}\text{Ti}_{0.5}\text{O}_3$ ,  $x=0.2$ . The data fit to the AT critical line predicted for an Ising spin-glass but (c) do not fit to the GT critical line.

disorder and magnetic frustration responsible for the spin glass-like behavior is not well understood. However, a possible conjecture is that some of the diamagnetic spin clusters involving  $\text{Ti}^{4+}$  ions could have been embedded in the ferromagnetic matrix involving  $\text{Fe}^{3+}$  ions because of the almost equal ionic radii and short-range ordering of these ions due to charge difference, causing the magnetic frustrations and randomness necessary for the origin of spin-glass behavior. The absence of spin-glass behavior for  $x \geq 0.3$  implies that La-doping has a significant role in affecting the magnetic

properties of the systems. However, further studies are needed to explore the role of La in tuning the magnetic properties.

It may be pointed out that because the  $B$ -site is randomly occupied by Ti and Fe with equal probability, the  $\text{Fe}^{3+}$  ion has, on average, only 3  $\text{Fe}^{3+}$  neighbors that can participate in the magnetic ordering. However, the nature of the magnetic interaction remains the same, i.e., each  $\text{Fe}^{3+}$  ion interacts magnetically with neighboring  $\text{Fe}^{3+}$  ions. Hence, due to the cooperative magnetic interaction of  $\text{Fe}^{3+}\text{-O-Fe}^{3+}$ , magnetic

ordering arises in this system.<sup>11</sup> The magnetic ordering temperature is the temperature at which the cooperative magnetic interaction sets in and forms a spin-network. However, above the magnetic ordering temperature, the spin network breaks, and consequently the cooperative magnetic interaction disappears. It can be pointed out that the magnetic interaction persists locally in magnetic clusters up to a certain critical temperature, above which the material becomes paramagnetic. We now discuss the effect of La-doping on the magnetic ordering. The magnetic ordering temperature is related to the average atomic distance of  $\text{Fe}^{3+}\text{-O-Fe}^{3+}$  along a-, b-, and c-crystallographic directions.<sup>11</sup> This implies that the longer the atomic distance, the lower the ordering temperature. In the case of the BLFPT<sub>x</sub> system, for  $x=0$ , the lattice parameter  $c$  of the tetragonal phase is larger than  $a$ , with a larger  $c/a$  than in other compositions. Thus, the average atomic distance of  $\text{Fe}^{3+}\text{-O-Fe}^{3+}$  along the  $c$ -direction is larger than that along the  $a$ - and  $b$ -directions. Therefore, the magnetic interaction along the  $c$ -direction weakens earlier than that along the  $a$ - and  $b$ -directions with increasing temperature, making the spin-network break. With an increase in  $x$ , the  $c/a$  ratio decreases, and hence the average

atomic distance along the  $c$  direction approaches that along the  $a$ -direction, which in turn enhances the magnetic ordering temperature. Therefore, an increase in the magnetic ordering temperature with increasing  $x$  is understandable.

#### D. Ferroelectric properties

Figure 11(a) shows the ferroelectric hysteresis loop of BLFPT<sub>x</sub> at ambient. Well-defined hysteresis loops were observed with increasing La-composition. However, the saturation of the polarization was not found to occur due to inadequate applied electric field. Note that the slope of the major axis of the hysteresis loop, which is proportional to the dielectric constant, increases rapidly in the tetragonal phase ( $x \leq 0.3$ ), suggesting that the dielectric response improves considerably as the anisotropy decreases. However, the remanent polarization remains low. One can also see that in the cubic phase (for  $x=0.4$  and  $0.5$ ) the loops at room temperature show a ferroelectric-like behavior with large remanent polarization, although the cubic phase is expected to be para-electric due to inversion symmetry. The variation of the remanent polarization as a function of composition is shown in Fig. 11(b). The remanent polarization increases with  $x$  rapidly in the cubic phase. Based on the shift of the peak temperature in  $\epsilon_r$  versus  $T$  plots, the cubic phase of BLFPT<sub>x</sub> has been shown to exhibit a relaxor behavior.<sup>14</sup> The relaxor behavior in the substituted system has been argued to arise from the formation of polar nano grains due to nano-scale ordering. This is also considered evidence of symmetry breaking, consistent with the observation of symmetry forbidden Raman scattering in the cubic phase. Thus, the present study of La-substitution in the multiferroic BF-PT system clearly establishes the manner in which the magnetic and dielectric properties are controlled by the tetragonal anisotropy of this system.

#### IV. CONCLUSION

Raman, magnetization, and polarization measurements were carried out on the single phase  $\text{Bi}_{1-x}\text{La}_x\text{FeO}_3\text{-PbTiO}_3$  ( $0 \leq x \leq 0.5$ ) system. The tetragonal anisotropy decreases considerably upon La-substitution, and the system turns cubic for  $x \geq 0.4$ . The Raman spectrum is found to become broad and weaker upon La-substitution. The Raman modes broaden further at elevated temperatures for all compositions. The temperature dependence of the mode frequencies shows a monotonic decrease, typical of anharmonic behavior. The discontinuous changes in the mode frequencies at 618 K in the sample with  $x=0.3$  is found to be associated with the tetragonal-cubic transition. In contrast to the expected broadening, two modes are found to become sharper at elevated temperature. This is believed to arise from a reduction of anisotropy in the system. The shape of the  $M$ - $H$  loops at low temperature suggests the existence of magnetically ordered clusters in an overall paramagnetic matrix. However, evidence of spin glass behavior is found in the compound with  $x=0.2$ . The dielectric response is found to increase with increasing La-composition in the tetragonal phase. The cubic phase exhibits relaxor behavior arising from the existence of polar nano regions.

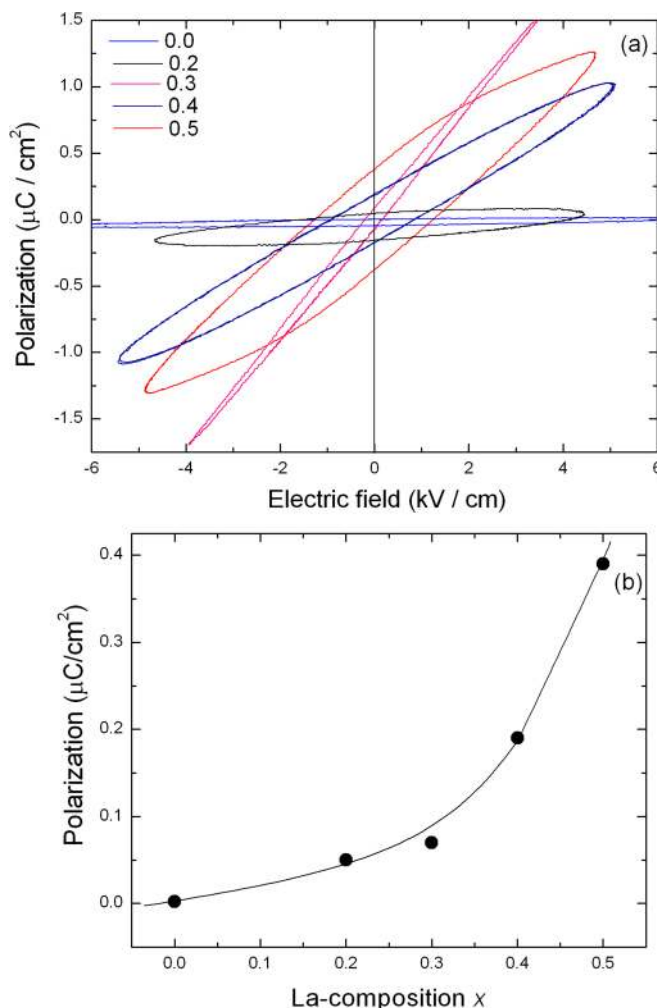


FIG. 11. (Color online) (a) Evolution of polarization ( $P$ - $E$ ) loop of  $(\text{Bi}_{1-x}\text{La}_x)_{0.5}\text{Pb}_{0.5}\text{Fe}_{0.5}\text{Ti}_{0.5}\text{O}_3$  ( $0 \leq x \leq 0.5$ ) at ambient temperature. (b) Effect of La-composition on the remanent polarization of BLFPT<sub>x</sub>. Curve through the data is a guide for the eye.

## ACKNOWLEDGMENTS

We acknowledge Mr. C. R. Das for EDAX analysis of the samples. We also acknowledge Ms. Shabana Khan for SAED analysis. We thank Dr. C. S. Sundar for interest in the work and Director IGCAR for encouragement.

- <sup>1</sup>Yu , N. Venevtsev, G. Zhdanov, and S. Solov'ev, *Sov. Phys. Crystallogr.* **4**, 538 (1960).
- <sup>2</sup>G. Smolenskii, V. Isupov, A. Agranovskaya, and N. Krainik, *Sov. Phys. Solid State* **2**, 2651 (1961).
- <sup>3</sup>F. Kubel and H. Schmid, *Acta Crystallogr., Sect. B: Struct. Sci.* **46**, 698 (1990).
- <sup>4</sup>M. M. Kumar, V. R. Palkar, K. Srinivas, and V. Suryanarayana, *Appl. Phys. Lett.* **76**, 2764 (2000).
- <sup>5</sup>S. T. Zhang, M. H. Lu, D. Wu, Y. F. Chen, and N. B. Ming, *Appl. Phys. Lett.* **87**, 262907 (2005).
- <sup>6</sup>X. Qi, J. Dho, R. Tomov, M. G. Blamire, and J. L. MacManus-Driscoll, *Appl. Phys. Lett.* **86**, 062903 (2005).
- <sup>7</sup>W. M. Zhu and Z.-G. Ye, *Ceram. Int.* **30**, 1435 (2004).
- <sup>8</sup>V. S. S. Sai Sunder, A. Halliyal, and A. M. Umarji, *J. Mater. Res.* **10**, 1301 (1995).
- <sup>9</sup>M. M. Kumar, A. Srinivas, S. V. Suryanarayana, and T. Bhimasankaram, *Phys. Status Solidi A* **165**, 317 (1998).
- <sup>10</sup>K. Balamurugan, N. H. Kumar, and P. N. Santhosh, *J. Appl. Phys.* **105**, 07D909 (2009).
- <sup>11</sup>W.-M. Zhu, H.-Y. Guo, and Z.-G. Ye, *Phys. Rev. B* **78**, 014401 (2008).
- <sup>12</sup>A. Singh, A. Gupta, and R. Chatterjee, *Appl. Phys. Lett.* **93**, 022902 (2008).
- <sup>13</sup>J. Cheng, S. Yu, J. Chen, and Z. Meng, *Appl. Phys. Lett.* **89**, 122911 (2006).
- <sup>14</sup>K. K. Mishra, V. Sivasubramanian, R. M. Sarguna, T. R. Ravindran, and A. K. Arora, *J. Solid State Chem.* **184**, 2381 (2011).
- <sup>15</sup>K. K. Mishra, R. M. Sarguna, S. Khan, and A. K. Arora, *AIP Advances* **1**, 032126 (2011).
- <sup>16</sup>N. K. Karan, R. S. Katiyar, T. Maiti, R. Guo, and A. S. Bhalla, *J. Raman Spectrosc.* **40**, 370 (2009).
- <sup>17</sup>J. Frantti and V. Lantto, *Phys. Rev. B* **56**, 221 (1997).
- <sup>18</sup>J. Frantti, V. Lantto, and J. Lappalainen, *J. Appl. Phys.* **79**, 1065 (1996).
- <sup>19</sup>A. Slodczyk, P. Daniel, and A. Kania, *Phys. Rev. B* **77**, 184114 (2008).
- <sup>20</sup>H. Zhang, S. Leppavuori, and P. Karjalainen, *J. Appl. Phys.* **77**, 2691 (1995).
- <sup>21</sup>P. S. Dabal, A. Dixit, and R. S. Katiyar, *J. Appl. Phys.* **89**, 8085 (2001).
- <sup>22</sup>C. Chemarin, N. Rosman, T. Pagnier, and G. Lucazeau, *J. Solid State Chem.* **149**, 298 (2000).
- <sup>23</sup>S. M. Cho and H. M. Jang, *Appl. Phys. Lett.* **76**, 3014 (2000).
- <sup>24</sup>M. N. Iiev, A. P. Litvinchuk, H.-G. Lee, C. L. Chen, M. L. Dezaneti, C. W. Chu, V. G. Ivanov, M. V. Abrashev, and V. N. Popov, *Phys. Rev. B* **59**, 364 (1999).
- <sup>25</sup>A. S. Bborovik-Romanov, *Sov. Phys. JETP* **11**, 786 (1960).
- <sup>26</sup>I. Sosnowska, R. Przenioslo, P. Fischer, and V. A. Murashov, *J. Magn. Mater.* **160**, 384 (1996).
- <sup>27</sup>R. Martinez, R. Palai, H. Huhtinen, J. Liu, J. F. Scott, and R. S. Katiyar, *Phys. Rev. B* **82**, 134104 (2010).
- <sup>28</sup>N. Waesermann, B. Mihailova, B. J. Maier, C. Paulmann, M. Gospodinov, V. Marinova, and U. Bismayer, *Phys. Rev. B* **83**, 214104 (2011).
- <sup>29</sup>M. D. Fontana, H. Idrissi, G. E. Kugel, and K. Wojcik, *J. Phys.: Condens. Matter* **3**, 8695 (1991).
- <sup>30</sup>A. K. Arora, D. U. Bartholomew, D. L. Peterson, and A. K. Ramdas, *Phys. Rev. B* **35**, 7966 (1987).
- <sup>31</sup>T. R. Ravindran, A. K. Arora, and T. A. Mary, *Phys. Rev. B* **67**, 064301 (2003).
- <sup>32</sup>R. Palai, H. Huhtinen, J. F. Scott, and R. S. Katiyar, *Phys. Rev. B* **79**, 104413 (2009).
- <sup>33</sup>M. Gruyters, *Phys. Rev. Lett.* **95**, 077204 (2005).
- <sup>34</sup>K. Binder and A. P. Young, *Rev. Mod. Phys.* **58**, 801 (1986).
- <sup>35</sup>K. H. Fischer and J. A. Hertz, *Spin Glasses* (Cambridge University Press, Cambridge, England, 1993).
- <sup>36</sup>J. B. Yi, J. Ding, Y. P. Feng, G. W. Peng, G. M. Chow, Y. Kawazoe, B. H. Liu, J. H. Yin, and S. Thongmee, *Phys. Rev. B* **76**, 224402 (2007).